Applied Clay Science 260 (2024) 107511

Contents lists available at ScienceDirect

Applied Clay Science

journal homepage: www.elsevier.com/locate/clay

Research Paper

Effects of salinity on the microscopic interaction and sedimentation behavior of halloysite nanotube

Yeong-Man Kwon [a,1], Namgyu Noh [b,1], Kyun-Seong Dae [b], Yusra Qureshi [b], Ji-Hwan Kwon [c], Gye-Chun Cho [d,*], Ilhan Chang [e,*], Jong Min Yuk [b,*]

[a] Department of Civil Engineering, Pukyong National University, 45 Yongso-ro, Nam-gu, Busan, 48513, Republic of Korea
[b] Department of Materials Science & Engineering, Korea Advanced Institute of Science and Technology, Daejeon 34141, Republic of Korea
[c] Interdisciplinary Materials Measurement Institute, Korea Research Institute of Standards and Science, Daejeon 34113, Republic of Korea
[d] Department of Civil and Environmental Engineering, Korea Advanced Institute of Science and Technology, Daejeon 34141, Republic of Korea
[e] Department of Civil Systems Engineering, Ajou University, Suwon-si 16499, Republic of Korea

ARTICLE INFO

Keywords:
Halloysite nanotube (HNT)
Salinity
Sedimentation
Flocculation
In-situ liquid-phase microscopy
DLVO theory

ABSTRACT

The response of clay minerals to changes in pore fluid salinity, particularly in coastal areas such as bays, lagoons, sounds, sloughs, and estuaries, has not been extensively studied. Herein, the influence of salinity exchange on the microscopic interaction and sedimentation behavior of halloysite nanotubes in an aqueous condition was investigated. In-situ microscopic observations and macro-scale sedimentation experiments reveal that halloysite nanotubes tend to disperse in pore fluids with high ionic strength because salt ions weaken the edge-to-face halloysite fabrics. Salinity exchange experiments demonstrate the permanent alteration of flocculation and sedimentation behavior due to the residual salt ions on the HNT surfaces. Even when the salt concentration is restored to its initial value, the presence of residual salts leads to the formation of a large and open floc structure, resulting in slower settling and a loosely packed final sediment. Our study provides a thorough understanding of the salt effect on sediment formation, including changes in the microscopic clay particle fabrics during salinity exchange.

1. Introduction

Dispersed clay particles flocculate and settle down in the solution state with gravitational and electrical forces (Kynch, 1952). The soil settling behavior is important for many practical applications such as stability of dispersions (Lisuzzo et al., 2019), separation strategies (Cavallaro et al., 2019), sediment accumulation (Watabe and Saitoh, 2015), reclamation (Kwon et al., 2019; Lee et al., 1987), disposal of mineral wastes (Zbik et al., 2008), river-floodplain morphodynamics (Lamb et al., 2020), colloidal chemistry (Lagaly and Ziesmer, 2003), and wastewater treatment (Shaikh et al., 2017). Various empirical and theoretical approaches have identified clay particle interaction mechanisms and sedimentation behaviors (Imai, 1980; Kwon et al., 2023a; Kwon et al., 2017; Kynch, 1952). It is known that complex parameters, such as particle size, sediment concentration, and organic and chemical environments, influence the settling behavior of clay particles in aqueous suspension (Berlamont et al., 1993; Chang and Cho, 2010; Kwon et al., 2023b). In general, greater particle size, container size, specific weight of sediment, and net particle attraction force cause sediments to settle faster, while higher particle hindrance and fluid viscosity conditions cause sediments to settle slower (Imai, 1980; Toorman, 1996).

As clay minerals have surface charge characteristics, the interaction and sedimentation behavior of clays are governed by net interparticle forces, i.e., double-layer force, van der Waals force and other forces described by the Derjaguin–Landau–Verwey–Overbeek (DLVO) theory

Abbreviations: HNT, halloysite nanotube; DLVO, Derjaguin–Landau–Verwey–Overbeek; EF, edge-to-face; FF, face-to-face; HHF, Hogg-Healy-Fuersteneau; LW, Lifshitz–van der Waals; EE, edge-to-edge; LPSEM, liquid-phase scanning electron microscopy; SiN_x, silicon nitride; LPTEM, liquid-phase transmission electron microscopy.

* Corresponding authors.
E-mail addresses: yeongman.kwon@pknu.ac.kr (Y.-M. Kwon), nnk1004@alumni.kaist.ac.kr (N. Noh), ddalgi1051@kaist.ac.kr (K.-S. Dae), yqureshi@kaist.ac.kr (Y. Qureshi), kwonjh@kriss.re.kr (J.-H. Kwon), gyechun@kaist.ac.kr (G.-C. Cho), ilhanchang@ajou.ac.kr (I. Chang), jongmin.yuk@kaist.ac.kr (J.M. Yuk).
[1] These authors contributed equally to the work and should be regarded as co-first authors.

https://doi.org/10.1016/j.clay.2024.107511
Received 13 November 2023; Received in revised form 24 July 2024; Accepted 24 July 2024
Available online 8 August 2024

(Missana and Adell, 2000; van Oss et al., 1990; Verwey, 1947). The chemical properties of the pore fluid (e.g., pH and salinity) have an impact on clay surface charges and net forces between clay particles (Durán et al., 2000; Kotylar et al., 1996; Sridharan and Prakash, 1999). Clay minerals are composed of a pH-independent or -dependent charge based on the protonation-deprotonation of broken bonds in the alumina layer (Mohan and Fogler, 1997; Tombácz and Szekeres, 2006). Because the edge surface is positively charged, clay particles prefer to form edge-to-face (EF) fabrics when the pH is below the isoelectric point of the edge surface (Rand and Melton, 1975; Rand and Melton, 1977). In contrast, the double-layer repulsion between all-negative clay surfaces regulates the clay interaction at a pH greater than the isoelectric point of the edge surfaces. Based on these findings, Wang and Siu (2006) observed a decrease in the settling velocity and an increase in the final sediment density with an increase in the pH of kaolinite suspensions.

Salt-induced double-layer compression affects the net interparticle forces. For example, as pore-fluid salinity increases, the repulsion force between two surfaces with identical charges tends to decrease (Israelachvili, 2011). In addition, salinity reduces the Coulomb attraction force between oppositely charged surfaces (Miklavic et al., 1994; Rand and Melton, 1977; Wang and Siu, 2006). On the other hand, van der Waals forces vary in a non-linear manner with the fluctuation in the dielectric constant of the pore media (Anandarajah and Chen, 1997; Chen and Anandarajah, 1998; Somasundaran et al., 2009). In other words, depending on the pore-fluid chemistry, the salinity strengthens or weakens particle attachments. Therefore, the surface charge heterogeneity of clay minerals makes it difficult to interpret the interactions between clay particles.

Recently, the direct observation technique has been used to reveal the underlying mechanism of particle interactions. In particular, liquid-phase microscopy is a powerful tool for elucidating the dynamical behavior between clay particles in a liquid, irrespective of the particle morphology, such as plates, spheres, rods, or nanotubes (Grogan et al., 2011; Liu et al., 2020; Ou et al., 2020; Sutter et al., 2016). However, the extensive analysis of the whole conformation process, from networking between individual particles to macro-scale floc association, is challenging due to the acceptable observable range of an individual liquid-phase microscopy technique.

Here, we aim to address an existing knowledge gap by directly visualizing the self-assembly behaviors of halloysite nanotubes (HNTs) in flocculation states using liquid-phase microscopy techniques. Furthermore, we analyzed the sedimentation behaviors of HNTs based on the observations made. Our findings unveiled previously hidden irreversible flocculation and sedimentation behaviors that correlate with the permanent double-layer compression that occurs during salinity exchange conditions. Based on the outcomes of this investigation, we established a relationship between clay mineral flocculation and sedimentation during temporal salinity exchange.

2. Material and methods

2.1. Sample information

HNTs sourced from various locations display differences in morphological properties like shape, length, size, and aspect ratio (Pasbakhsh et al., 2013), all of which can affect their settling behavior (Du et al., 2010; Komar and Reimers, 1978). This study utilized HNTs (CAS: 1332-58-7; Sigma-Aldrich, St. Louis, MO, USA) without undergoing additional purification (Fig. 1a) with a median particle size of 6 μm (Fig. S1). HNTs are distinguished by their unique microstructure, with diameters of 10–30 nm and lengths between 500 and 1500 nm. HNTs carry a high surface area and porosity due to the presence of alumina and silica layers (Fahimizadeh et al., 2024; Niu et al., 2023; Deshmukh et al., 2023). HNTs share the same structure and chemical composition as clays of the kaolinite group, and unlike kaolinite, which has a platy shape, they have a tubular form that is more suited for liquid cell microscope observation. The tubular structure of HNTs allows for more uniform dispersion and less interference with the observation of individual particles. This enhanced dispersion facilitates clearer imaging and more accurate analysis of particle interactions and sedimentation behavior. They had a broad distribution in weathered rocks and tropical and subtropical areas (Massaro et al., 2020). HNTs were chosen as the focus of this investigation due to their potential as nanocontainers with controlled-release capabilities (Lazzara et al., 2018). The tubular morphologies of dried HNT particles (Fig. 1b, c) were confirmed using a scanning electron microscope, SEM (SU5000; Hitachi, Tokyo, Japan), and a transmission electron microscope, TEM (JEM-3010; JEOL, Tokyo, Japan). Element mapping analysis (Fig. 1d) was performed to confirm the composition of dried HNT by using JEM-ARM200CF (JEOL, Tokyo, Japan) equipped with energy-dispersive X-ray (EDX) detectors. The zeta potential of the HNT suspension in deionized water, with a measured pH of 4.5, was determined to be −22 mV using a particle analyzer (Litesizer 500; Anton Paar, Graz, Austria), consistent with Vergaro et al. (2010).

2.2. In-situ liquid microscopy

HNT powders were fractionated to investigate the microscopic interactions using in-situ electron microscopy with the gravitational

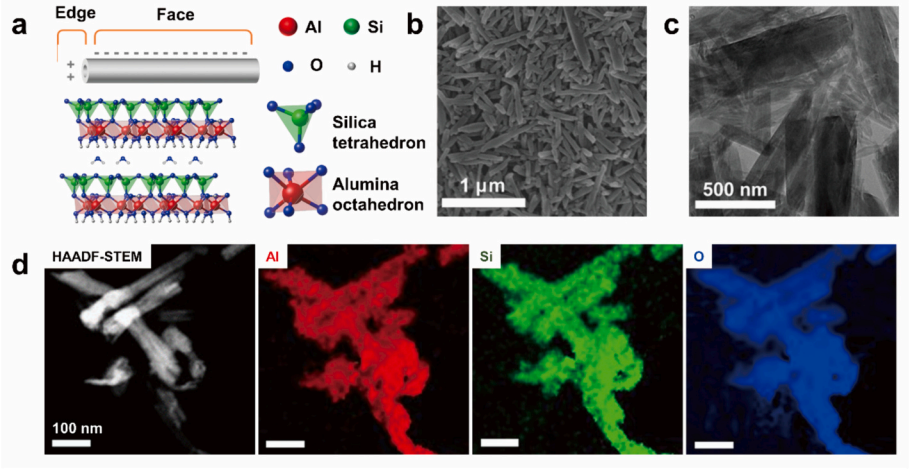

Fig. 1. The structure and settling behavior of halloysite nanotubes. (a) Schematic diagram of the halloysite nanotube (HNT) structure. (b) scanning electron microscope (SEM) image, and (c) transmission electron microscope (TEM) image of dried HNT. (d) High-angle annular dark-field scanning transmission electron microscopy (HAADF-STEM) image and chemical composition maps of Al, Si, and O of HNT particles.

methods developed by Jackson (Jackson and Barak, 2005), which help filter agglomerated particles >2 μm. Then, to obtain the monodispersed suspension, filtered HNTs were dispersed in water (10 mM) using a tip-sonicator, the VCS-750 (Sonics & Materials, Inc., Newtown, CT, USA). To differentiate the individual particles in confinement, we used a low concentration in suspension, which provides the initial flocculation behavior.

To investigate the microscopic insights into the associations of HNTs, we introduced in-situ liquid cell microscopy systems, which enabled us to record the time-series events of the flocculation formation and particle association change in response to a change in the solution environment and salinity. A TEM equipped with the USC1000 (Gatan, Inc., Warrendale, PA, USA) camera and a Poseidon holder (Protochips, Morrisville, NC, USA) was used to observe the real-time liquid-phase TEM (LPTEM) measurements at an acceleration voltage of 300-kV. The liquid chamber equipped in the Poseidon holder consisted of a SiN_x membrane-based liquid cell with ~50 nm height and 2 × 2 mm^2 space. HNTs were infused into the liquid holder system to resolve the flocculation process from a particulate point of view using the Pump 11 Elite Syringe Pumps (Harvard Apparatus, Holliston, MA, USA), with an infusion rate of 0.5 μL/min (Sigma 300; Carl Zeiss Meditec, Inc., Baden-Württemberg, Germany).

A homemade liquid-cell SEM holder was used to visualize the flocculation behavior at different salinity levels. The chamber dimension of LPSEM is ~1 μm in height and 2 × 2 mm^2 space. The silicon nitride (SiN_x)-based liquid flowing system can provide the initial settling stage through the injection of dispersed particles. We gathered a series of snapshots corresponding to the different salinities: 0.01, 0.1, 0.3, and 0.6 M. Sodium chloride (NaCl), the most abundant salt in seawater, was used to prepare fluids with different salinity conditions by dissolving 99.5% pure NaCl (CAS: 7647-14-5; Junsei Chemical Co., Ltd., Tokyo, Japan) in deionized water.

For monitoring HNT aggregates under the salinity exchange condition, we used liquid-phase optical microscopy, LPOM (Olympus, Tokyo, Japan). It was observed after the suspension was dropped onto the glass slide at each salinity value after salinity exchange from salination (from 0.01 to 0.6 M) to desalination (from 0.6 to 0.01 M).

2.3. Sedimentation experiment for clay suspensions

The HNT fabrics of suspension with high water content (a percentage by weight of the water compared to the total weight of the soil, [1000%]) were assessed from the sedimentation behavior, measured with time from the initial suspension stage until the HNT sediment reached a constant volume. A graduated cylinder (60 mm in diameter and a maximum volume of 1000 mL) was filled with 100 mL of the test fluid. HNTs (90 g; 35 mL in volume) were poured into the cylinder with 100 mL of test fluid and mixed to form a condensed suspension. Then, additional test fluid was poured into the cylinder to reach a final volume of 935 mL. The HNT suspension was slowly mixed by shaking upside down until a uniform suspension was obtained. The prepared suspensions were rested for 24 h for complete hydration. A thermoplastic film (Parafilm M; Bermis Company, Inc., Bellwood, IL, USA) capped the top of the cylinders for sealing and wrapping. Then, fully hydrated HNT suspensions were vigorously disturbed for at least 1 min by shaking and inverting each sealed cylinder upside down. The cylinders were placed on a level surface after the last inversion, which was regarded as the commencement of sedimentation (time = 0). The sediment height was tracked over time until the final sediment height reached a constant volume with a settlement rate of <1.0 mL/day. A single sedimentation period could last up to 7 days.

The study encompassed experiments under two distinct salinity regimes. For the initial condition, a static salinity environment was maintained, wherein the supernatant was treated with NaCl at concentrations of 0, 0.01, 0.3, and 0.6 M. The second condition examined the dynamics of salinity fluctuations, which arise in various practical scenarios such as physical changes in water masses, biological absorption, chemical buffering, dissolution, precipitation, evaporation, dilution, ice melting, groundwater discharge, aeolian contributions, and ocean mixing (Lebrato et al., 2020). After the sediment stabilized at a consistent height (i.e., a settlement rate of <1.0 mL/day), the overlying supernatant was carefully decanted using a pipette (Model: WI.5.381.000, Witeg, Wertheim, Germany). Subsequently, the cylinder was replenished to a volume of 935 mL using a fluid with an altered salinity concentration, facilitated by a pipette. During this phase, the salinity was systematically modulated, commencing from at 0 and escalating incrementally through 0.01, 0.1, 0.3, and 0.6 M (i.e., salination). Following this, a stepwise reduction in salinity was instituted, proceeding from 0.3 M to 0.1 M, 0.01 M, and culminating at 0 M NaCl (i.e., desalination).

3. Results and discussion

3.1. Fundamental flocculation behavior among HNTs

In-situ LPTEM has been performed to demonstrate the fundamental formation pathways of floc fabrics at an earlier stage. We tracked the newly formed fabrics over the entire infusion experiment. Fig. 2a and Video 1 show the real-time LPTEM images of the flocculation events between HNT particles in the suspension. Basically, a pairing of HNTs is initiated by the attachment of the injected particles. The supplied particles are directly contacted at the edge or face of the preformed objects. The floc structures initiated by attachments of HNTs and EE/EF-based associations increase continuously with increasing injection time (Fig. 2b). The assembly of HNTs is primarily governed by van der Waals forces and electrostatic attractions (Prinz Setter and Segal, 2020), which preferentially favor the EE and EF structures due to their energy efficiency in minimizing the net interaction energy as shown in Fig. 2c, d (Theng and Wells, 1995). A double-contacted structure can form to minimize the net interaction energy, which can be permitted for the floc-to-floc assembly process (Fig. 2e).

Meanwhile, the separated particles, which have moved away from their original bound states, can transfer to a new contact state with nearby particles. Face-to-face (FF) assembly is rarely observed due to the repulsive field between double layers with identical charges (Chen et al., 2015). The majority of microstructures exhibit a complex architecture mainly composed of edge-to-edge (EE) and edge-to-face (EF) associations (Fig. S2), which have been proposed as common mechanisms for creating clay networks (Zbik et al., 2008). The aggregates, developed outside the viewing area by the long infusion length, directly attach the preformed assembly with multiple EE and EF connections. Therefore, the floc size grew because of the attachment processes. The particle interaction is efficiently regulated to minimize the net interaction energy in the liquid system, according to these dynamic processes of HNTs. By consecutive particle and floc attachment in the settling stage, multidimensional HNT frameworks are created.

3.2. Salinity effect on flocculation behavior among HNTs

To visualize the sedimentation behavior in HNT suspension, we facilitated in-situ liquid-phase scanning electron microscopy (LPSEM). Fig. 3a shows the floc formation of the HNTs in suspensions at different initial salinity conditions. At low salinity, the HNT building blocks assemble to form a large aggregate. Although the floc shapes are atypical, the microstructure of aggregates consists of HNT networks, mainly with unit EE and EF associations. In contrast, the projected floc areas decrease from ~2.6 $μm^2$ to ~0.5 $μm^2$ as salinity increased from 0.01 to 0.6 M (Fig. 3b). The HNT networks in the floc are significantly reduced. This decrease in floc size with increasing salinity can be attributed to the compression of the electrical double layer around each particle, significantly reducing the range and magnitude of electrostatic interactions between HNTs. The observed formation of HNT flocs is associated with

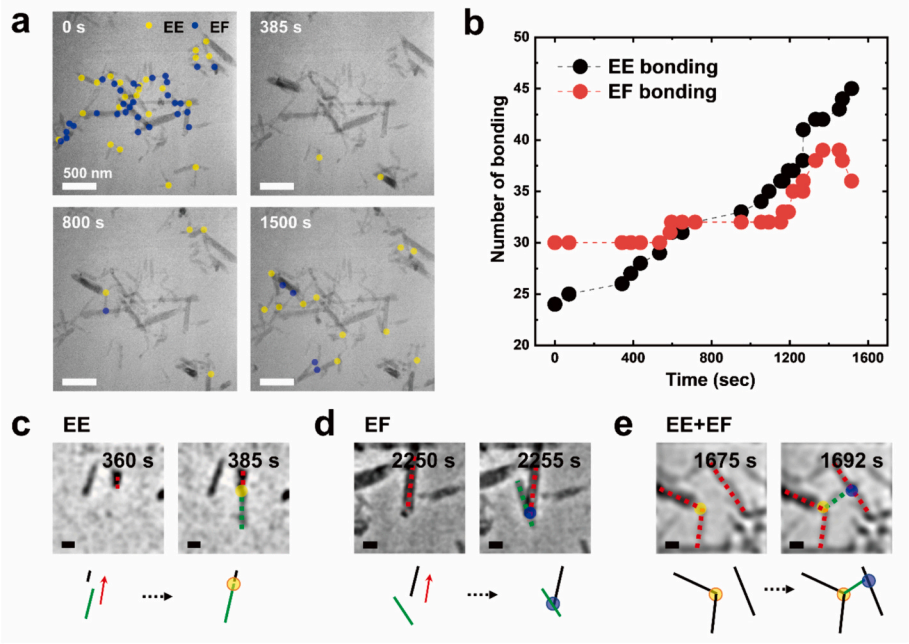

Fig. 2. Halloysite nanotube (HNT) interactions and possible flocculation pathways in pure water. (a) Initial flocculation process of the individual HNTs identified using in-situ LPTEM at $t = 0$, 385, 800, and 1500 s. Yellow and blue dots indicate the newly formed EE and EF association points, respectively. (b) Population of the EE and EF associations of preformed floc extracted from projected TEM images. (c–e) Sequential TEM images and schematic diagrams of particular HNT assemblies for time-dependent HNT interaction in pure liquid. In most cases, (c) edge-to-edge (EE), (d) edge-to-face (EF), and (e) both formation processes by direct attachment of individual HNT particles (EE + EF). Red dotted lines represent the pre-existing particle, and green dotted lines represent the attached particles. The scale bars in c–e represent 100 nm. (For interpretation of the references to colour in this figure legend, the reader is referred to the web version of this article.)

the sedimentation behavior of HNTs at different salinities (Fig. 3c). Higher salinity resulted in a lower initial settling rate and dense final sediment (Fig. 3d), which aligns with prior findings that settling is impeded in saline water (Cao et al., 2018; Liu et al., 2018). These sedimentation features are well explained by net interaction forces in a colloidal system with NaCl additives (Fig. 3e, Table S1, and Fig. S3). In the salinity increase cases, all particle interaction is suppressed by double-layer compression (Palomino and Santamarina, 2005). Notably, salt addition effectively reduced the attraction between oppositely charged clay surfaces (EF attraction; Fig. S3b). These results show that HNTs with higher salinity become more dispersive and are stacked by FF fabrics (Fig. S3a), resulting in the formation of dense final sediment (Watabe and Saitoh, 2015). Consequently, the reduction in floc size induced by salt ions leads to a slower progression of sedimentation.

3.3. HNT interactions at the salinity exchange conditions

To demonstrate the effect of salinity exchange on initial flocculation, we performed liquid-phase optical microscopy (LPOM) via a series of salination (0.01 M → 0.1 M → 0.3 M → 0.6 M) and desalination (0.6 M → 0.3 M → 0.1 M → 0.01 M) exchange procedures (Fig. 4a). After most of the particles settled down in droplets, macro-scale aggregated HNTs were observed. With increasing salinity, the average floc diameter decreases from 7 μm to 6.1 μm. During the desalination process, suspended particles may assemble with each other as an increasing double layer on the periphery of the HNT. With decreasing salinity, the floc sizes increase from 6.1 μm to 7.7 μm (Fig. 4b).

We consider the role of salt in the colloid to explain these phenomena (Fig. 4c). Na^+ ion has a low affinity with silica tetrahedrons of HNT surface in low ionic strength, and it only forms a broad diffusion layer on the periphery of HNTs. However, Na^+ ions can create a dense ionic cloud on a negatively charged surface with an increase in salt to 0.6 M NaCl (Katana et al., 2020). The Na^+ ion prefers to be directly linked to the silica tetrahedron outer sphere or defective sites of HNT with high ionic strength (Li et al., 2015), causing permanent screening of the surface charge of HNT.

Due to the directly coupled structure with the outer HNT surface, the salt ions adhering to the surface are not completely removed when the salt concentration is lowered. As salinity is reduced, the residual Na^+ ions remain bound to the HNT surface, causing a sustained disruption in the electrostatic balance (Luckham and Rossi, 1999). This weakens the EF interaction more significantly than the EE interaction, as the latter relies more on van der Waals forces, which are less influenced by ionic strength (Liu et al., 2018). The role of salinity in altering the structural configuration of HNT aggregates is further elucidated by observing the changes in the aggregate structure during the salinity exchange process. This dynamic interaction highlights how changes in ionic conditions can lead to a permanent alteration in the flocculation behavior of HNTs. The EE interaction formed a honeycomb structure with the largest pore volume (i.e., lower density) in aggregate structure compared to the EF-induced structure. These results indicate that the residual salt ions on the HNT surfaces are effectively worked into the particle-to-particle interaction by pore salinity variation. In other words, salinity changes in the colloidal systems might permanently alter the initial flocculation and sedimentation structures of HNT minerals.

The sedimentation experiments were conducted within a step-by-step liquid replacement setup, mimicking the changes in salinity seen in LPOM (as shown in Fig. S4–6). Every sample showed a decrease in sediment height over time, which reached a stable level before 72 h. The initial settling rate experienced a slight increase during the desalination phase, yet it did not return to the original rate corresponding to each distinct salinity level (Fig. 4d). This underscores the previously discussed phenomenon, where remaining salt ions on HNT surfaces play a crucial role in adjusting loose aggregation during shifts in salinity. The development of loose aggregates also led to a reduction in the final sediment density during desalination when compared to the same salinity condition during salination (Fig. 4e). This underscores the notion that alterations in salinity within colloidal systems can have a persistent influence on the fundamental structure of flocculation and sedimentation in HNT minerals.

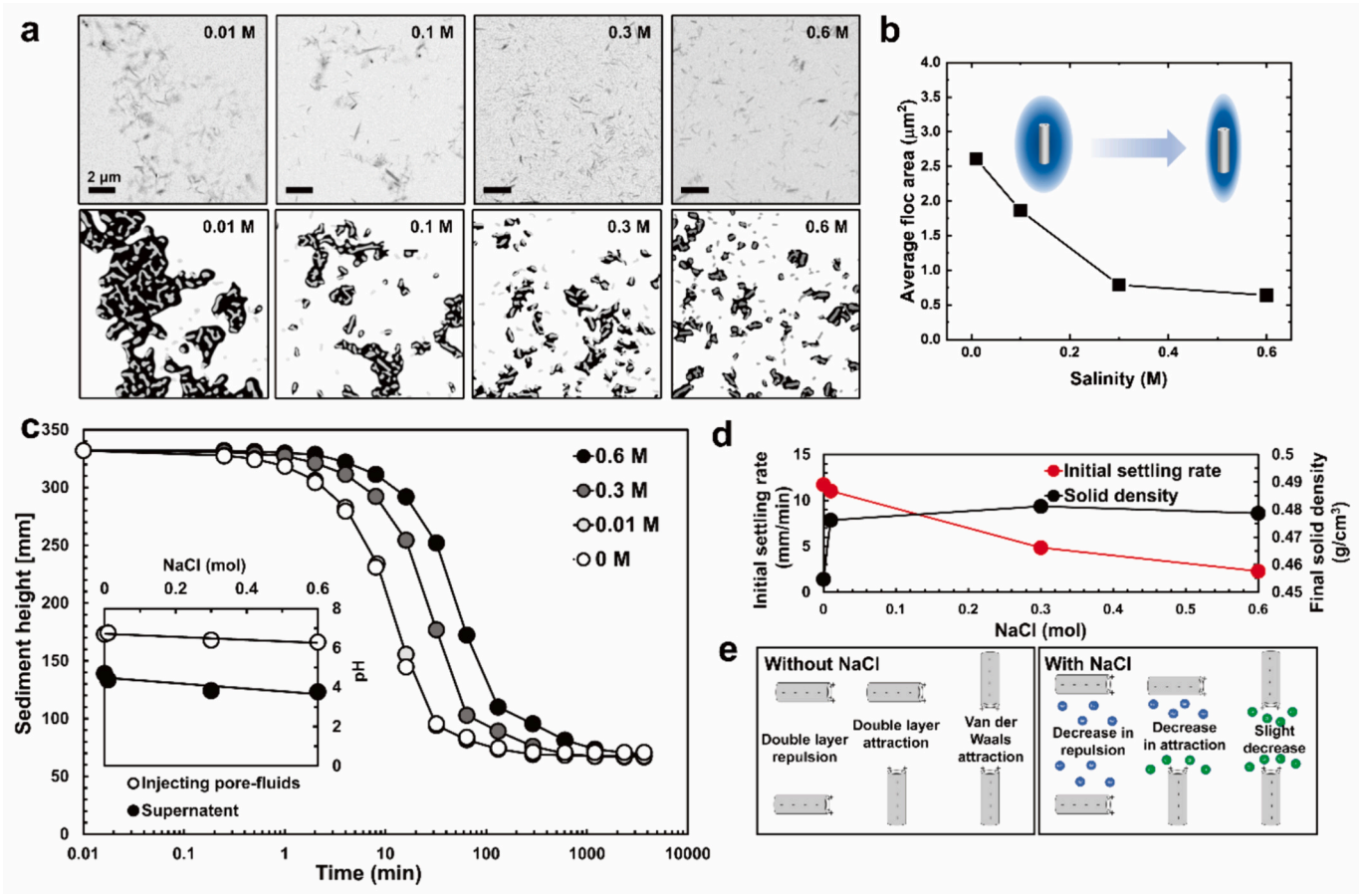

Fig. 3. The sedimentation behavior of halloysite suspensions varies depending on the salinity levels. (a) Microscopic structures of the flocculated HNTs observed using in-situ liquid-phase scanning electron microscopy (LPSEM). The upper panels are representative SEM images at individual salinities (0.01, 0.1, 0.3, and 0.6 M), and the lower panels are processed images corresponding to the upper SEM images. (b) Average floc area extracted from processed SEM images at different salinity levels. (c) The variation in sediment height, (d) the initial settling rate and final sediment density during sedimentation. (e) The schematic description of the dominant interparticle force between face-to-face, edge-to-face, and edge-to-edge surfaces.

4. Conclusion

Multiscale analysis was used to explore the sedimentation behavior and interparticle interaction of HNTs affected by salinity exchange, which included in-situ liquid-phase microscopic observations and sedimentation tests of soil mass. At low salinity, the HNTs assemble by Coulombic (EF association with opposite charge) and van der Waals (EE association) attraction to minimize net interaction energies. It forms large aggregates with card house structures composed of EF-dominant densely packed structures. Thus, the aggregates result in a higher settling velocity.

The double-layer field of HNTs is compressed by concentrated salt ions as salinity increases, and particle interaction is effectively suppressed. Hence, decreased particle contact can reduce the aggregate size and cause particle dispersion during settling. In contrast, when salt concentrations with low ionic strength are recovered, the Na^+ ions are not completely removed from the HNT surface and may induce persistent compression of the double layer field of the face side. As a result, the microfloc structures are transformed into loosely packed EE-dominant honeycomb structures, which can lead to forming a larger and more open floc. As a result of the variations in microstructure induced by the remaining salt, the settling speed becomes slower, and the sediments are more open and low-density than in the original conditions.

The combination of in-situ liquid-phase microscopy techniques provided the entire observation, from initial flocculation to the final sedimentation of clay minerals in salted solution. Our findings revealed the crucial role of clay minerals and salt additives in the correlation of flocculation and sedimentation behaviors in a liquid environment. The salt additives provide a suppression nature of clay mineral interaction. As the salinity is adjusted, it creates a change in the permanent charge configuration at the clay mineral surfaces, which is one of the most important aspects of comprehending the fundamental mechanisms that govern the micro- and macro-structure of natural clay minerals as salinity varies. The interaction features of clay nanoparticles may bring new insight into controlling the electrochemical or physical properties of clay minerals for specific applications. The result has the potential to drive progress in the analysis of sedimentation patterns of clay minerals, encompassing areas such as pharmaceutical drug delivery, tissue engineering scaffolds, wastewater treatment, dredging, optimization of nutrient delivery to plants, and land reclamation procedures. Further study should be conducted to explore the physicochemical interactions and sedimentation behavior of HNTs in various natural and industrial settings, considering the range of cations present.

Supplementary data to this article can be found online at https://doi.org/10.1016/j.clay.2024.107511.

Funding

This research was financially supported by the National Research Foundation (NRF) of Korea (Grants No. 2022R1A2C2091517, 2023R1A2C300559611, 2022R1A2C2008929).

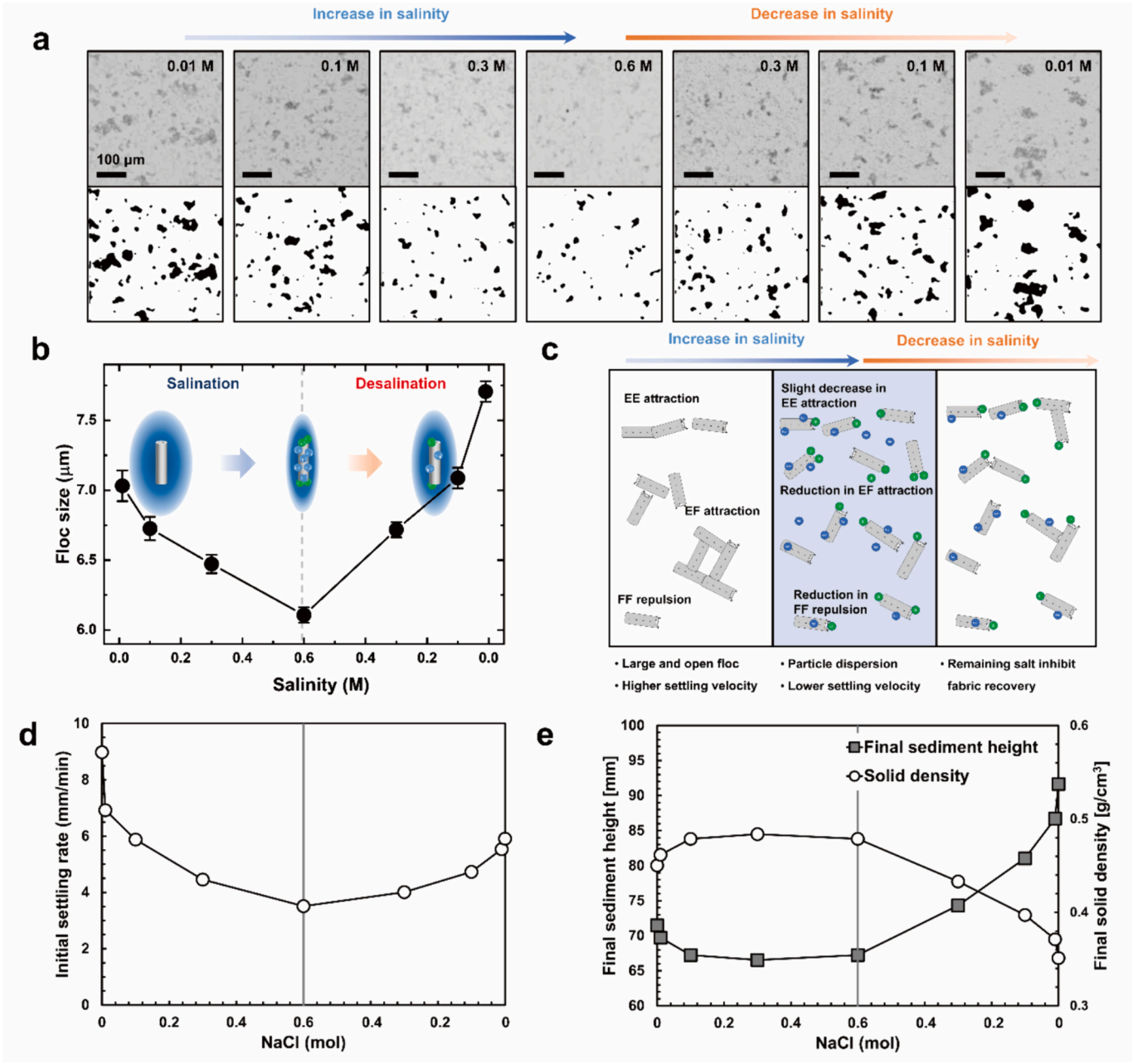

Fig. 4. Aggregate formation via a series of salination and desalination processes. (a) Serial liquid-phase optical microscopy (LPOM) images of conglomerated fabrics during the change in condition from salination (0.01 to 0.6 M) to desalination (0.6 to 0.01 M). Upper panels are representative OM images, and lower panels are processed images corresponding to upper OM images, respectively. (b) The aggregate area with changes in salinity extracted from processed OM images. (c) The summary of particle interaction via a series of salination and desalination. Blue and green spheres indicate the Na^+ and Cl^- ions, respectively. The response of (d) the initial settling rate and (e) the final sediment density to changing salinity conditions. (For interpretation of the references to colour in this figure legend, the reader is referred to the web version of this article.)

CRediT authorship contribution statement

Yeong-Man Kwon: Writing – review & editing, Writing – original draft, Methodology, Formal analysis, Data curation, Conceptualization. **Namgyu Noh:** Writing – review & editing, Writing – original draft, Methodology, Formal analysis, Data curation, Conceptualization. **Kyun-Seong Dae:** Writing – review & editing, Writing – original draft, Validation, Methodology, Formal analysis, Conceptualization. **Yusra Qureshi:** Writing – review & editing. **Ji-Hwan Kwon:** Writing – review & editing, Methodology, Investigation, Data curation, Conceptualization. **Gye-Chun Cho:** Writing – review & editing, Methodology, Investigation, Data curation, Conceptualization. **Ilhan Chang:** Writing – review & editing, Supervision, Formal analysis, Conceptualization. **Jong Min Yuk:** Writing – review & editing, Supervision, Formal analysis, Conceptualization.

Declaration of competing interest

The authors declare the following financial interests/personal relationships which may be considered as potential competing interests:

Jong Min Yuk reports financial support was provided by National Research Foundation of Korea. If there are other authors, they declare that they have no known competing financial interests or personal relationships that could have appeared to influence the work reported in

this paper.

Data availability

All necessary data generated or analyzed during this study are included in this published article, and other auxiliary data are available from the corresponding authors upon request.

Acknowledgments

We thank Editage (www.editage.co.kr) for English language editing.

References

Anandarajah, A., Chen, J., 1997. Van Der Waals attractive force between clay particles in water and contaminants. Soils Found. 37, 27–37.
Berlamont, J., Ockenden, M., Toorman, E., Winterwerp, J., 1993. The characterisation of cohesive sediment properties. Coast. Eng. 21, 105–128.
Cao, J., Kang, X., Bate, B., 2018. Microscopic and physicochemical studies of polymer-modified kaolinite suspensions. Colloids Surf. A Physicochem. Eng. Asp. 554, 16–26.
Cavallaro, G., Lazzara, G., Taormina, V., Cascio, D., 2019. Sedimentation of halloysite nanotubes from different deposits in aqueous media at variable ionic strengths. Colloids Surf. A Physicochem. Eng. Asp. 576, 22–28.
Chang, I., Cho, G.C., 2010. A new alternative for estimation of geotechnical engineering parameters in reclaimed clays by using shear wave velocity. Geotech. Test. J. 33, 171–182.
Chen, J., Anandarajah, A., 1998. Influence of pore fluid composition on volume of sediments in kaolinite suspensions. Clay Clay Miner. 46, 145–152.
Chen, Q., Cho, H., Manthiram, K., Yoshida, M., Ye, X., Alivisatos, A.P., 2015. Interaction potentials of anisotropic nanocrystals from the trajectory sampling of particle motion using in situ liquid phase transmission electron microscopy. ACS Cent. Sci. 1, 33–39.
Deshmukh, R.K., Kumar, L., Gaikwad, K.K., 2023. Halloysite nanotubes for food packaging application: a review. Appl. Clay Sci. 234, 106856.
Du, J., Morris, G., Pushkarova, R.A., St, C., Smart, R., 2010. Effect of surface structure of kaolinite on aggregation, settling rate, and bed density. Langmuir 26, 13227–13235.
Durán, J.D.G., Ramos-Tejada, M.M., Arroyo, F.J., González-Caballero, F., 2000. Rheological and electrokinetic properties of sodium montmorillonite suspensions: I. Rheological properties and interparticle energy of interaction. J. Colloid Interface Sci. 229, 107–117.
Fahimizadeh, M., Wong, L.W., Baifa, Z., Sadjadi, S., Auckloo, S.A.B., Palaniandy, K., Pasbakhsh, P., Tan, J.B.L., Singh, R.K.R., Yuan, P., 2024. Halloysite clay nanotubes: innovative applications by smart systems. Appl. Clay Sci. 251, 107319.
Grogan, J.M., Rotkina, L., Bau, H.H., 2011. In situ liquid-cell electron microscopy of colloid aggregation and growth dynamics. Phys. Rev. E 83, 061405.
Imai, G., 1980. Settling behavior of clay suspension. Soils Found. 20, 61–77.
Israelachvili, J.N., 2011. Intermolecular and Surface Forces, 3rd ed. Academic press, London.
Jackson, M.L.R., Barak, P., 2005. Soil Chemical Analysis: Advanced Course. UW-Madison Libraries Parallel Press, USA.
Katana, B., Takacs, D., Csapo, E., Szabo, T., Jamnik, A., Szilagyi, I., 2020. Ion specific effects on the stability of halloysite nanotube colloids-inorganic salts versus ionic liquids. J. Phys. Chem. B 124, 9757–9765.
Komar, P.D., Reimers, C.E., 1978. Grain Shape Effects on Settling rates. J. Geol. 86, 193–209.
Kotylar, L.S., Sparks, B.D., Schutte, R., 1996. Effect of salt on the flocculation behavior of nano particles in oil sands fine tailings. Clay Clay Miner. 44, 121–131.
Kwon, Y.-M., Im, J., Chang, I., Cho, G.-C., 2017. ε-Polylysine biopolymer for coagulation of clay suspensions. Geomech. Eng. 12, 753–770.
Kwon, Y.-M., Chang, I., Lee, M., Cho, G.-C., 2019. Geotechnical engineering behaviors of biopolymer-treated soft marine soil. Geomech. Eng. 17, 453–464.
Kwon, Y.-M., Chang, I., Cho, G.-C., 2023a. Consolidation and swelling behavior of kaolinite clay containing xanthan gum biopolymer. Acta Geotech. 18, 3555–3571.
Kwon, Y.-M., Kang, S.-J., Cho, G.-C., Chang, I., 2023b. Effect of microbial biopolymers on the sedimentation behavior of kaolinite. Geomech. Eng. 33, 121–131.
Kynch, G.J., 1952. A theory of sedimentation. Trans. Faraday Soc. 48, 166–176.
Lagaly, G., Ziesmer, S., 2003. Colloid chemistry of clay minerals: the coagulation of montmorillonite dispersions. Adv. Colloid Interf. Sci. 100, 105–128.
Lamb, M.P., de Leeuw, J., Fischer, W.W., Moodie, A.J., Venditti, J.G., Nittrouer, J.A., Haught, D., Parker, G., 2020. Mud in rivers transported as flocculated and suspended bed material. Nat. Geosci. 13, 566–570.
Lazzara, G., Cavallaro, G., Panchal, A., Fakhrullin, R., Stavitskaya, A., Vinokurov, V., Lvov, Y., 2018. An assembly of organic-inorganic composites using halloysite clay nanotubes. Curr. Opin. Colloid Interface Sci. 35, 42–50.
Lebrato, M., Garbe-Schönberg, D., Müller, M.N., Blanco-Ameijeiras, S., Feely, R.A., Lorenzoni, L., Molinero, J.-C., Bremer, K., Jones, D.O.B., Iglesias-Rodriguez, D., Greeley, D., Lamare, M.D., Paulmier, A., Graco, M., Cartes, J., Barcelos e Ramos, J., de Lara, A., Sanchez-Leal, R., Jimenez, P., Paparazzo, F.E., Hartman, S.E., Westernströer, U., Küter, M., Benavides, R., da Silva, A.F., Bell, S., Payne, C., Olafsdottir, S., Robinson, K., Jantunen, L.M., Korablev, A., Webster, R.J., Jones, E. M., Gilg, O., Bailly du Bois, P., Beldowski, J., Ashjian, C., Yahia, N.D., Twining, B., Chen, X.-G., Tseng, L.-C., Hwang, J.-S., Dahms, H.-U., Oschlies, A., 2020. Global variability in seawater Mg:Ca and Sr:Ca ratios in the modern ocean. Proc. Natl. Acad. Sci. 117, 22281–22292.
Lee, S.L., Karunaratne, G.P., Yong, K.Y., Ganeshan, V., 1987. Layered clay-sand scheme of land reclamation. J. Geotech. Eng. 113, 984–995.
Li, X., Li, H., Yang, G., 2015. Promoting the adsorption of metal ions on kaolinite by defect sites: a molecular dynamics study. Sci. Rep. 5, 14377.
Lisuzzo, L., Cavallaro, G., Parisi, F., Milioto, S., Lazzara, G., 2019. Colloidal stability of halloysite clay nanotubes. Ceram. Int. 45, 2858–2865.
Liu, D., Edraki, M., Berry, L., 2018. Investigating the settling behaviour of saline tailing suspensions using kaolinite, bentonite, and illite clay minerals. Powder Technol. 326, 228–236.
Liu, Z., Zhang, Z., Wang, Z., Jin, B., Li, D., Tao, J., Tang, R., De Yoreo, J.J., 2020. Shape-preserving amorphous-to-crystalline transformation of CaCO3 revealed by in situ TEM. Proc. Natl. Acad. Sci. USA 117, 3397–3404.
Luckham, P.F., Rossi, S., 1999. The colloidal and rheological properties of bentonite suspensions. Adv. Colloid Interf. Sci. 82, 43–92.
Massaro, M., Noto, R., Riela, S., 2020. Past, present and future perspectives on halloysite clay minerals. Molecules 25.
Miklavic, S.J., Chan, D.Y., White, L.R., Healy, T.W., 1994. Double-layer forces between heterogeneous charged surfaces. J. Phys. Chem. 98, 9022–9032.
Missana, T., Adell, A., 2000. On the applicability of DLVO theory to the prediction of clay colloids stability. J. Colloid Interface Sci. 230, 150–156.
Mohan, K.K., Fogler, H.S., 1997. Effect of pH and layer charge on formation damage in porous media containing swelling clays. Langmuir 13, 2863–2872.
Niu, W., Qui, X., Wu, P., Guan, W., Zhan, Y., Jin, L., Zhu, N., 2023. Unrolling the tubes of halloysite to form dickite and its application in heavy metal ions removal. Appl. Clay Sci. 231, 106748.
Ou, Z., Wang, Z., Luo, B., Luijten, E., Chen, Q., 2020. Kinetic pathways of crystallization at the nanoscale. Nat. Mater. 19, 450–455.
Palomino, A.M., Santamarina, J.C., 2005. Fabric map for kaolinite: effects of pH and ionic concentration on behavior. Clay Clay Miner. 53, 211–223.
Pasbakhsh, P., Churchman, G.J., Keeling, J.L., 2013. Characterisation of properties of various halloysites relevant to their use as nanotubes and microfibre fillers. Appl. Clay Sci. 74, 47–57.
Prinz Setter, O., Segal, E., 2020. Halloysite nanotubes – the nano-bio interface. Nanoscale 12, 23444–23460.
Rand, B., Melton, I.E., 1975. Isoelectric point of the edge surface of kaolinite. Nature 257, 214–216.
Rand, B., Melton, I.E., 1977. Particle interactions in aqueous kaolinite suspensions: I. Effect of pH and electrolyte upon the mode of particle interaction in homoionic sodium kaolinite suspensions. J. Colloid Interface Sci. 60, 308–320.
Shaikh, S.M.R., Nasser, M.S., Hussein, I., Benamor, A., Onaizi, S.A., Qiblawey, H., 2017. Influence of polyelectrolytes and other polymer complexes on the flocculation and rheological behaviors of clay minerals: a comprehensive review. Sep. Purif. Technol. 187, 137–161.
Somasundaran, P., Mehta, S.C., Yu, X., Krishnakumar, S., 2009. Colloid Systems and Interfaces Stability of Dispersions through Polymer and Surfactant Adsorption. CRC Press, Boca Raton, FL.
Sridharan, A., Prakash, K., 1999. Influence of clay mineralogy and pore-medium chemistry on clay sediment formation. Can. Geotech. J. 36, 961–966.
Sutter, E., Sutter, P., Tkachenko, A.V., Krahne, R., de Graaf, J., Arciniegas, M., Manna, L., 2016. In situ microscopy of the self-assembly of branched nanocrystals in solution. Nat. Commun. 7, 11213.
Theng, B.K.G., Wells, N., 1995. The flow characteristics of halloysite suspensions. Clay Miner. 30, 99–106.
Tombácz, E., Szekeres, M., 2006. Surface charge heterogeneity of kaolinite in aqueous suspension in comparison with montmorillonite. Appl. Clay Sci. 34, 105–124.
Toorman, E.A., 1996. Sedimentation and self-weight consolidation: general unifying theory. Géotech 46, 103–113.
van Oss, C.J., Giese, R.F., Costanzo, P.M., 1990. DLVO and non-DLVO interactions in hectorite. Clay Clay Miner. 38, 151–159.
Vergaro, V., Abdullayev, E., Lvov, Y.M., Zeitoun, A., Cingolani, R., Rinaldi, R., Leporatti, S., 2010. Cytocompatibility and uptake of halloysite clay nanotubes. Biomacromolecules 11, 820–826.
Verwey, E.J.W., 1947. Theory of the stability of lyophobic colloids. J. Phys. Colloid Chem. 51, 631–636.
Wang, Y.H., Siu, W.K., 2006. Structure characteristics and mechanical properties of kaolinite soils. I. Surface charges and structural characterizations. Can. Geotech. J. 43, 587–600.
Watabe, Y., Saitoh, K., 2015. Importance of sedimentation process for formation of microfabric in clay deposit. Soils Found. 55, 276–283.
Zbik, M.S., Smart, R.S.C., Morris, G.E., 2008. Kaolinite flocculation structure. J. Colloid Interface Sci. 328, 73–80.